Spin wave dynamics and the determination of intrinsic damping in locally-excited Permalloy thin films

Zhigang Liu,[*] Fabian Giesen, Xiaobin Zhu,[†] Richard D. Sydora, and Mark R. Freeman

Department of Physics, University of Alberta, Edmonton, AB T6G 2G7, Canada

Time-resolved scanning Kerr effect microscopy has been used to study magnetization dynamics in Permalloy thin films excited by transient magnetic pulses generated by a micrometer-scale transmission line structure. The results are consistent with magnetostatic spin wave theory and are supported by micromagnetic simulations. Magnetostatic volume and surface spin waves are measured for the same specimen using different bias field orientations and can be accurately calculated by k-space integrations over all excited plane wave components. A single damping constant of Gilbert form is sufficient to describe both scenarios. The nonuniform pulsed field plays a key role in the spin wave dynamics, with its Fourier transform serving as a weighting function for the participating modes. The intrinsic Gilbert damping parameter α is most conveniently measured when the spin waves are effectively stationary.

Interest has been growing for many years in the time-domain investigation of magnetization dynamics in response to a short magnetic pulse. An impulse excitation is broadband, but the dynamics of the magnetic system are also very sensitive to the parameters of the excitation pulse. Time-domain pulse shaping can eliminate ringing for a coherently-switched ferromagnetic element, to greatly enhance the performance for applications [1, 2]. In addition, the spatial profile of the pulsed field is critical in dictating the magnetic dynamics. Magnetostatic spin waves generated by such nonuniform transient field have been observed in a number of time-resolved optical [3] and inductive [4, 5] experiments, and also in frequency-domain studies [6]. The resulting position-dependent temporal response creates additional challenges for characterizing the dynamics and for determining the intrinsic magnetic damping. The focus of the present work is to address these difficulties within a simple physical framework.

Under the condition of linear behavior of the spin wave dynamics in the low amplitude regime [4, 5], the magnetic response is the linear superposition of all plane wave components that can be excited by the pulse. Assuming the spin waves propagate only along the x direction (the coordinate system is defined in Fig.1(a)), the out-of-plane component of magnetization can be described by:

$$ M_z(x,t) = e^{-\frac{t}{\tau}} \int_0^{k_c} P(k, \omega(k)) \sin[kx - \omega(k)t + \phi] dk \quad (1) $$

where τ^{-1} is the inverse decay time, $\omega(k)$ is the dispersion relation, and $P(k, \omega(k))$ is the spectral density of the pulse field determined from its spatial and temporal profiles and acts as a relative weighting factor for the different spin wave components in k-space. The influences of the pulse field parameters, the intrinsic damping, and the dispersion relation of the spin waves are contained explicitly. k_c is a cut-off wave number for numerical integration ($k_c = 5 \ \mu m^{-1}$ is sufficient for the magnetostatic

regime with the stripline dimensions used here). The initial phase angle ϕ is taken to be independent of frequency on account of the pulse excitation. The longer trailing edge of the pulse causes a non-oscillatory quasi-static background that is not included in Eq.(1), but in actual calculations we take the pulse shape into account by fitting the high-frequency data [7].

The experimental geometry is shown by the inset schematics in Fig.1. A $Ni_{80}Fe_{20}$ film (Permalloy, or "Py"), with thickness $d = 10 \pm 1$ nm, is deposited on a 150 μm thick glass substrate using e-beam evaporation. The film is then clamped on a copper thin film stripline, with a small amount of high-vacuum dielectric grease applied for a strong surface-tension bond and to ensure electrical isolation between Py and Cu. Two coplanar wires in the stripline structure transmit a current pulse (rise time < 20 ps at the sample) from a semi-insulating GaAs photoconductive switch (carrier lifetime ~ 300 ps) and generate a nonuniform magnetic pulse $\boldsymbol{h}(x,t)$. The width and separation of the wires are both 3 μm and are much smaller than the length ($\sim 400 \ \mu m$), and the system can be treated as quasi-one-dimensional. The pulse field amplitude (and corresponding initial torque) decreases quickly away from the wires, falling to less than 10% of the peak value beyond $|x| = 8 \ \mu m$ for the experimental geometry. We define the region of the Py film enclosed by these boundaries as the "source" area. An in-plane bias field $\boldsymbol{H}_0$ saturates the magnetization of the Py film such that $\boldsymbol{M}_0$ is parallel to $\boldsymbol{H}_0$. This layout fixes the directions of the wave vectors $\boldsymbol{k}$ to be parallel to x-axis, and enables us to detect different spin wave modes by changing the direction of $\boldsymbol{H}_0$ ($\boldsymbol{M}_0$). The focus here is on the special cases of $\boldsymbol{k} \parallel \boldsymbol{M}_0$ and $\boldsymbol{k} \perp \boldsymbol{M}_0$, although other angles can be similarly addressed [8]. Changes of M_z are measured by means of time-resolved scanning Kerr effect microscopy [9]. This technique offers ~ 500 nm spatial resolution determined by the spot size of the focused probe beam (much smaller than typical spin wave length

encountered in this work), and introduces a versatility relative to the pulsed inductive method, whose spatial resolution is limited by fixed-position, micrometer-size probe devices, and suffers a loss of signal when the magnetization is perpendicular to the wires. The optical approach allows a direct determination of a variety of spin wave dispersion laws.

Quasi-1D micromagnetic modeling was also carried out in order to benchmark the k-space calculation. The magnetic film was discretized along the x-direction, such that the "finite elements" were 10 nm in both x- and z-directions, while infinitely long in y-direction. The spin motion of each element obeys the Landau-Lifshitz-Gilbert (LLG) equation [10]:

$$\frac{d\boldsymbol{M}}{dt} = -\gamma_0 \boldsymbol{M} \times \boldsymbol{H}_{\text{eff}} + \frac{\alpha}{M_s} \boldsymbol{M} \times \frac{d\boldsymbol{M}}{dt} \qquad (2)$$

where $\gamma_0 = 17.61$ MHz/Oe is the gyromagnetic ratio, $M_s = 760$ emu/cm^3 is the saturation magnetization of the Permalloy film, and α is the Gilbert damping parameter. $\boldsymbol{H}_{\text{eff}}$ is the effective field mainly contributed by the external field and the magnetostatic field. The exchange interaction is found to be insignificant in the magnetostatic regime [4, 11]. The implementation of the simulation follows standard procedures [10, 12].

Fig.1(a) shows the typical response of M_z, in the $\boldsymbol{k} \parallel \boldsymbol{M}_0$ geometry, with $H_{0x} = 200$ Oe. The solid curve is a measurement at $x = 0$, and other positions show almost the same profile but with amplitude decrease with increasing x. The damping is spatially uniform and not influenced by the propagation of spin waves [13, 14], consistent with expectation for $\boldsymbol{k} \parallel \boldsymbol{M}_0$. This geometry exhibits magnetostatic backward volume waves with a dispersion law [15]:

$$\omega^2 = \omega_H^2 + \omega_H \omega_M (1 - e^{-kd})/kd \qquad (3)$$

where $\omega_H = \gamma_0 H_0$, $\omega_M = 4\pi\gamma_0 M_s$. For the present experiments, the group velocity, $v_g = \frac{d\omega}{dk}$, is on the order of 0.1 μm/ns and the spin waves are effectively stationary over the time scale of the measurement. The calculated waveform based upon Eq.(1) is plotted by the crosses in Fig.1(a), and agrees well with the measured data. To determine the weighting function $P(k, \omega(k))$, a standard linearization analysis is applied on Eq.(2) [16] to give $M_z = \frac{\omega_M \omega_H}{\omega_H^2 - \omega^2} h(\omega) h_z(k)$, where $h(\omega)$ and $h_z(k)$ are the Fourier transformation of $h(t)$ and $h_z(x)$, respectively. The ω-dependent quantities are found to be insignificant in the calculations (except for a negative sign if $\omega > \omega_H$), so the weighting function can be approximated by $P(k) = |h_z(k)|$. The Biot-Savart law was used to calculate the in-plane (h_x) and out-of-plane (h_z) components of the excitation field. The spatial distributions of h_x and h_z depend on the distance Δ between the plane of the Py film and the plane of the stripline. Δ cannot be precisely measured here and is used as a fitting parameter. In this nearly stationary case, magnetic damping
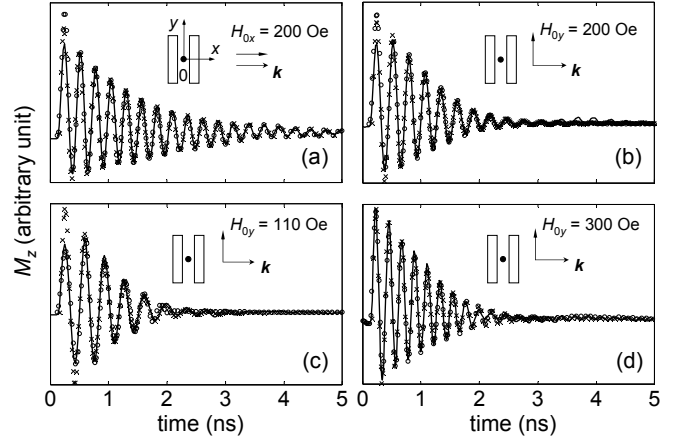

FIG. 1: Different damping behavior of local magnetization under nonuniform excitation. The coordinate system is defined in (a) and is the same throughout the work. The parallel rectangular bars represent the stripline structure and the black dots represent the probe points (not to scale). Relation between the wave vector and the bias field is shown in each panel. The solid curves are measured $M_z(t)$ traces, the crosses are calculated results based on Eq.(1), and the open circles are simulated results using the quasi-1D LLG model [17].

of the system is unambiguously determined by the exponential decay time τ in Eq.(1), and can be measured directly from the logarithm of the decreasing amplitude of the experimental waveform; the result for Fig.1(a) is $\tau = 1.40 \pm 0.01$ ns. On the other hand, the Gilbert damping parameter α can be independently fitted by micromagnetic simulations based solely on LLG equation; the result for this case is $\alpha = 0.0081 \pm 0.0003$, and the simulated waveform is plotted by open circles in Fig.1(a), in excellent correspondence with the measurement and the k-space calculation. The two damping parameters are related by $\tau = [\alpha\gamma_0(2\pi M_s + H_0)]^{-1}$ [16], and our results obtained by independent fittings are consistent with this relation.

Good agreement between the measurements, k-space calculations, and quasi-1D simulations are again obtained in the $\boldsymbol{k} \perp \boldsymbol{M}_0$ geometry, as shown in Fig.1(b-d) for the probe positioned at $x = 0$ and H_{0y} ranging from 110 Oe to 300 Oe. In this geometry magnetostatic surface waves (MSSW) are the dominant modes, leading to qualitatively different spatiotemporal dynamics in the Py film. For the k-space calculations, the dispersion law of MSSW [16, 18, 19],

$$\omega^2 = (\omega_H + \omega_M/2)^2 - (\omega_M/2)^2 \exp(-2kd) \qquad (4)$$

is used to calculate $M_z(x, t)$ using Eq.(1). Linear response theory for the surface modes yields $M_z = \frac{\omega_M}{\omega_H^2 - \omega^2} h(\omega)[\omega_H h_z(k) + i\omega h_x(k)]$, that is, the out-of-plane magnetization responds to both in-plane and out-of-plane pulse fields. In the present work $\omega_H \ll \omega$, the contribution of h_z is small and the weighting function again

can be approximated by $P(k) = |h_x(k)|$ [20] (the ⟨
dependence is neglected as in the $\boldsymbol{k} \parallel \boldsymbol{M}_0$ case). Th
$M_z(t)$ traces show significantly shortened decay tim
(compare Fig.1(b) to Fig.1(a)), since the excited surfa
modes possess fairly large group velocity to transfer th
nonequilibrium spin wave energy out of the probed pos
tion. At $x = 0$, the decay time shown in Fig.1(b-d) do
not change explicitly when H_{0y} decreases (which leads
increasing group velocity), but after we average $M_z(x,$
over $|x| \leqslant 8$ μm, the decay time in the whole "sourc
area indeed decreases with larger group velocity, as e
pected (results not shown). In other words, the dam
ing behavior in MSSW configuration cannot be quantit
tively described by single-point measurements, but has
be analyzed using the global approaches (scanning prol
experiment, micromagnetic simulation and k-space calc
lation). The damping behavior is naturally embedded
Eq.(1), because of dephasing of the component freque
cies through the $\omega(k)t$ term. Eq.(1) is a generalization
the formula proposed in Ref.[4], which gives an intuiti
description of the phenomenon. The damping envelope
is jointly determined by a Gaussian term accounting for
spin wave dispersion, and the intrinsic exponential de-
cay. Our general approach works for both $\boldsymbol{k} \parallel \boldsymbol{M}_0$ and
$\boldsymbol{k} \perp \boldsymbol{M}_0$ geometries, and explains why the decay remains
exponential when the spin wave propagation is negligible.

In the $\boldsymbol{k} \perp \boldsymbol{M}_0$ geometry, individual wave packets
propagating in the x direction can be observed when
$M_z(t)$ is measured outside the "source" area (i.e., the
probe point moves away from the stripline). Represen-
tative results for the case of $H_{0y} = 80$ Oe are shown in
Fig.2(a-d). Recording a two dimensional (position and
time) map for the peak of the wave packet, its group
velocity can be determined to be 4.8 ± 0.5 μm/ns. Per-
forming such analysis for a range of bias fields yields the
group velocity as a function of frequency, as shown in
Fig.2(e). The measurements and numerical calculations
agree reasonably well with the MSSW theory (v_g deter-
mined from Eq.(4)).

For the propagating wave packet discussed above, the
$M_z(t)$ is asymmetric in time (the increase of the os-
cillation amplitude appears "slower" than the follow-
ing decline). This asymmetry is especially apparent
in Fig.2(c,d), but again is well reproduced by the k-
space calculation based on Eq.(1) (and which cannot be
achieved by the Gaussian-type formula in Ref.[4]). This is
shown by the crosses in Fig.2(a-d), and is also supported
by the quasi-1D simulations (open circles). A single scale
factor fits the measured amplitude at all positions in the
considered range, indicating that the Gilbert mechanism
($\alpha = 0.0081$ is still used here [21]) also accounts for the
spin wave attenuation during propagation [4, 13]. Mea-
surements of this attenuation are potentially an effective
way to determine α when $\boldsymbol{k} \perp \boldsymbol{M}_0$.

The temporal profile of $M_z(t)$ ultimately stems from
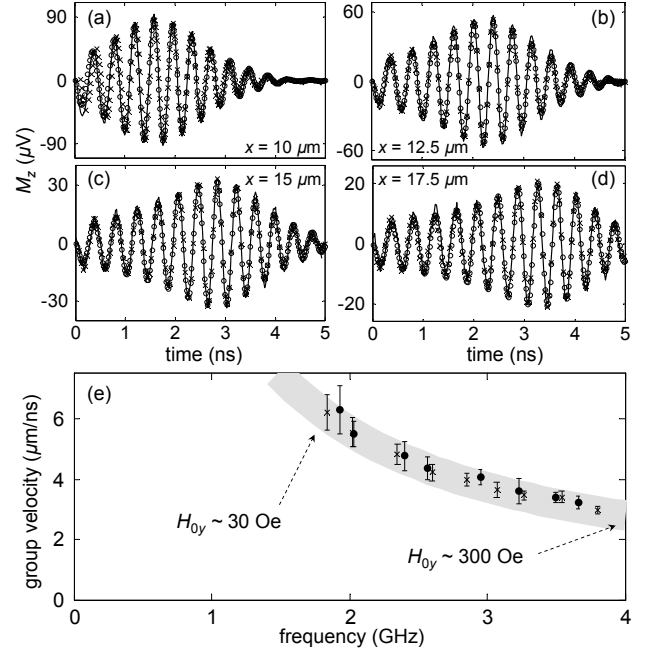the spatial profile of the excitation field, which directly

FIG. 2: Propagation of a spin wave packet in the $\boldsymbol{k} \perp \boldsymbol{M}_0$
geometry. (a) – (d): $M_z(t)$ traces at $x = 10$, 12.5, 15 and
17.5 μm, respectively, when $H_{0y} = 80$ Oe. The solid curves
represent the measured data, which are extracted from a sin-
gle spatiotemporal scan, the crosses are the calculated results
based on Eq.(1), and the open circles are the simulated re-
sults using the quasi-1D LLG model. The simulated and cal-
culated waveforms are scaled to the same amplitude as the
experimental data. (e): Group velocity of MSSW modes as a
function of oscillation frequency, with H_{0y} ranging from 30 to
300 Oe. The black dots are measured data, and the crosses
are results from quasi-1D simulations. The grey shadow is
the theoretical curve calculated from MSSW dispersion law
(Eq.(4)), with the width reflecting its lower and upper lim-
its due to the uncertainty in the cutoff wavelength and film
thickness ($k = 0 \sim 5$ μm^{-1} and $d = 9 \sim 11$ nm).

determines $P(k)$ in Eq.(1). Fig.3 illustrates the effect of
different distributions $P(k)$, calculated for several values
of the film-stripline gap Δ. As Δ increases, the spatial
variation of the pulse field becomes smoother and $P(k)$
acquires relatively higher spectral density at smaller k
(Fig.3(a)). This yields relatively larger oscillation ampli-
tude at early times before the wave packet peaks, and can
be understood here as a consequence of more spin wave
components with higher phase velocity $v_p = \frac{\omega}{k}$. Figs.3(b-
d) show the bracketing of the "best-fit", $\Delta = 1.6$ μm, to
the experimental data as presented in Fig.2(d).

As the spin wave packet propagates farther away from
the source, its shape is gradually broadened and the peak
time eventually exceeds the maximum optical delay of
the apparatus (5 ns). In this situation, the oscillations
are dominated by small-k components. The experiments
yield a unique position at each bias field ($x \sim 30$ μm for
the case of $H_{0y} = 80$ Oe) where the incoming energy from
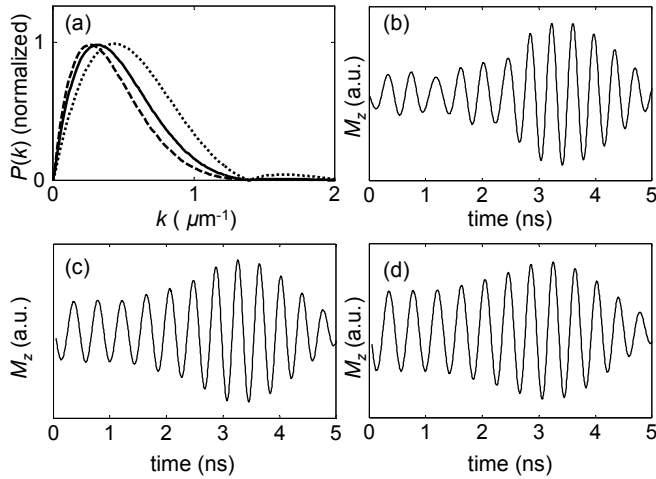the propagating mode effectively balances the intrinsic

FIG. 3: Influence of the spatial distribution of the pulse field. (a), Calculated distributions of normalized $P(k)$ for $\Delta = 0.5$ μm (dotted curve), $\Delta = 1.6$ μm (solid curve), and $\Delta = 2.5$ μm (dashed curve). (b) – (d), $M_z(t)$ traces at $x = 17.5$ μm calculated with Eq.(1), using $\Delta = 0.5$ μm, $\Delta = 1.6$ μm, and $\Delta = 2.5$ μm, respectively.
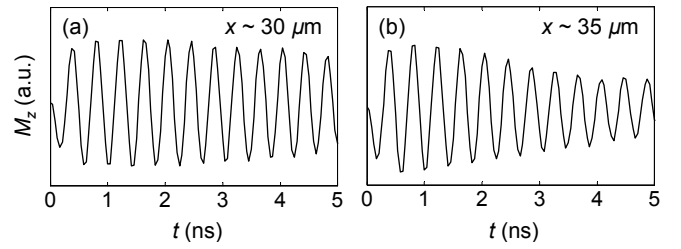
FIG. 4: Spin wave oscillations measured at (a), $x \sim 30$ μm and (b), $x \sim 35$ μm. The experimental conditions are the same as those in Fig.2(a-d).

dissipation at that position, such that a nearly time-independent oscillation amplitude is observed throughout the measurement window, as shown in Fig.4(a). For larger x, the power balance is broken and the intrinsic decay of the long-wavelength oscillations dominates (Fig.4(b)).

In summary, we have studied the spatiotemporal dynamics of a ferromagnetic film in response to a short magnetic pulse localized in one spatial dimension. The response can be interpreted as a superposition of plane waves modulated by the spectral densities of the spatially nonuniform, transient excitation field, and decaying according to intrinsic Gilbert damping. Magnetostatic volume modes and surface modes can be self-consistently described within this interpretation, and the experimental and analytical results show good agreement also with micromagnetic simulations. The Gilbert damping parameter could be directly measured from broadband FMR waveforms when the spin waves are effectively stationary. The k-space calculations also require negligible computer resources in comparison to micromagnetic simulations, and offer an opportunity to invert the problem and design magnetic waveforms for applications. In addition, the analysis can be extended to a second dimension to account for thicker or multilayered structures, or for 2D spin wave propagation.

* Electronic address: zgliu@Phys.UAlberta.CA
† Present address: Seagate Research, 1251 Waterfront Place, Pittsburgh, PA 15222

[1] Th. Gerrits, H. A. M. van den Berg, J. Hohlfeld, L. Bär and Th. Rasing, Nature **418**, 509 (2002).
[2] H. W. Schumacher, C. Chappert, P. Crozat, R. C. Sousa, P. P. Freitas, J. Miltat, J. Fassbender, and B. Hillebrands, Phys. Rev. Lett. **90**, 017201 (2003).
[3] T. J. Silva, M. R. Pufall, and Pavel Kabos, J. Appl. Phys. **91**, 1066 (2002).
[4] M. Covington, T. M. Crawford, and G. J. Parker, Phys. Rev. Lett., **89**, 237202 (2002).
[5] M. Wu, B. Kalinikos, P. Krivosik, and C. E. Patton, J. Appl. Phys., **99**, 013901 (2006).
[6] S. Tamaru, J. A. Bain, R. J. M. van de Veerdonk, T. M. Crawford, M. Covington, and M. H. Kryder, Phys. Rev. B, **70**, 104416 (2004).
[7] A. Y. Elezzabi and M. R. Freeman, Appl. Phys. Lett. **68**, 3546 (1996).
[8] F. Giesen *et al.*, to be published.
[9] W. K. Hiebert, A. Stankiewicz, and M. R. Freeman, Phys. Rev. Lett., **79**, 1134 (1997).
[10] J. Miltat, G. Albuquerque, and A. Thiaville, in *Spin dynamics in confined magnetic structures I*, edited by B. Hillebrands and K. Ounadjela (Springer, New York, 2002).
[11] T. M. Crawford, M. Covington, and G. J. Parker, Phys. Rev. B **67**, 024411 (2003).
[12] M. Mansuripur, J. Appl. Phys. **63**, 5609 (1988).
[13] M. Bailleul, D. Olligs, and C. Fermon, Appl. Phys. Lett. **83**, 972 (2003).
[14] A. Barman, V. V. Kruglyak, R. J. Hicken, J. M. Rowe, A. Kundrotaite, J. Scott, and M. Rahman, Phys. Rev. B **69**, 174426 (2004).
[15] M. Bailleul, D. Olligs, C. Fermon, and S. O. Demokritov, Europhys. Lett. **56**, 741 (2001).
[16] A. G. Gurevich and G. A. Melkov, *Magnetization Oscillations and Waves*, (CRC Press, New York, 1996).
[17] The model pulse shape gives rise to a mismatch over the first cycle of oscillation as measured at the center of the transmission lines. This does not affect the conclusions concerning damping. The propagating spin wave packets measured outside the transmission line structure are insensitive to this detail of the pulse shape.
[18] G. M. Sandler, H. N. Bertram, T. J. Silva, and T. M. Crawford, J. Appl. Phys. **85**, 5080 (1999).

[19] R. W. Damon and J. R. Eshbach, J. Phys. Chem. Solids., **19**, 308, (1961).

[20] $|h_x(k)|$ and $|h_z(k)|$ have the same profile.

[21] Fitting to the data for surface waves is more complicated than for volume waves due to stronger dispersion, and result in a larger uncertainty. The fitting quality is in the same level for $\alpha = 0.0081 \pm 0.0006$.